Marine and Petroleum Geology 135 (2022) 105385

Contents lists available at ScienceDirect

Marine and Petroleum Geology

journal homepage: www.elsevier.com/locate/marpetgeo

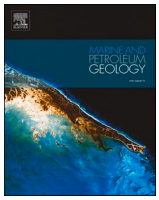

Trace element variations across Middle–Upper Cambrian carbonates: Implications for the paleoenvironment of eastern Laurentia

Noel C. Shembilu *, Karem Azmy

Department of Earth Sciences, Memorial University of Newfoundland, St. John's, NL, A1B 3X5, Canada

ARTICLE INFO

Keywords:
Middle-upper cambrian carbonates
Paleoenvironment
Dolomicrites
Redox conditions
Eastern laurentia
Western newfoundland (Canada)

ABSTRACT

The investigated Middle–Upper Cambrian carbonates span, from bottom to top, the uppermost Hawke Bay (40 m), the March Point (~83 m thick), and the lowermost Petit Jardin (~47 m) formations of the Port au Port Group (western Newfoundland, Canada). A multi-technique evaluation of the preservation of carbonates was applied by using several petrographic and chemical screening tools. The variations in several proxies of bioproductivity (e.g., P, Ni, and Cu), input of weathering products (Mn, Fe, Al, and ∑REE), and paleoredox (e.g., Th/U) have been utilized to study the paleoenvironmental conditions during the investigated time interval. Distinct positive shifts in the profiles of Al, ∑REE, Mn, and Fe have been associated with the negative shifts recorded by the $\delta^{13}C$ profile and correlated with the DICE (Middle Cambrian) and base of the SPICE (lowermost Upper Cambrian) events. They reflect contributions from detrital weathered material during sealevel falls. Similar correlated positive shifts are also documented by the P, Ni, and Cu profiles, thus suggesting an increase in the riverine inputs of nutrients associated with the drop of sealevel and increase of weathering activities. In addition, the changes in the bioproductivity and weathering proxies were associated with relative rising in the Th/U ratios (0.1–8.3), which reflects variations in the redox state towards relatively more oxidizing conditions.

1. Introduction

The Cambrian Period represents the critical stage of evolution of life in the oceans and the appearance of first shelly organisms in the Phanerozoic seawater (e.g., Babcock et al., 2015; Buatois et al., 2016; LeRoy et al., 2021). Lime mudstones are abundant in the Cambrian carbonate successions and have been widely used for global chemostratigraphic correlations (e.g., Derry et al., 1992; Kaufman et al., 1993; Veizer et al., 1999; Hill and Walter, 2000; McKirdy et al., 2001). Preservation of marine carbonates is the foundation for the reconstruction of paleoenvironmental conditions that dominated during the Earth's history (Wignall and Twitchett, 1996; Veizer et al., 1999). Micritic carbonates, including dolomicrites, have been found at times to retain their near-primary geochemical signatures (e.g., Land, 1992; Chang et al., 2021; Liang and Jones, 2021; Liyuan et al., 2021).

The eustatic sealevel variations during the Late Cambrian influenced the redox conditions and organic primary productivity as well as the terrestrial inputs of weathered material into the oceans, which also affected the contents of trace elements, including total rare-earth elements (∑REE), in the ocean water and the deposited marine carbonates (e.g., Wignall and Twitchett, 1996; Arnaboldi and Meyers, 2007). Thus, the eustasy causes variations in the elemental compositions of the marine carbonates such as those of P, Si, Al, U, Ni, Cu and ∑REE (e.g., Arnaboldi and Meyers, 2007; Wignall et al., 2007; Wang and Azmy, 2020) and also lead to changes in the redox conditions, which is reflected by the relative changes in the Th/U ratios (e.g., Sholkovitz and Shen, 1995; Wignall and Twitchett, 1996; Kimura et al., 2005).

The March Point Formation constitutes the lowest part of the Port au Port Group and is formed of mixed shales, sandstones, and carbonates (Chow and James, 1987, 1992). These sedimentary rocks might be organic-rich enough to become a source that can constitute a part of a hydrocarbon system if some of the carbonate interbeds are porous and sealed by non-porous overlying sediments particularly when shales from neighboring basins are, to some extent, organic rich (Weaver and Macko, 1988). However, no evaluation, even preliminary, of the organic contents of the Port au Port Group shales has been documented yet. Therefore, understanding the paleoenvironment and redox conditions during the precipitation of the investigated carbonates will shed light on the main conditions that dominated during the deposition of the entire succession.

* Corresponding author.
E-mail address: ncs361@mun.ca (N.C. Shembilu).

https://doi.org/10.1016/j.marpetgeo.2021.105385
Received 16 April 2021; Received in revised form 15 October 2021; Accepted 16 October 2021
Available online 21 October 2021

The main objectives of this study are:

i. To investigate the influence of sealevel changes on trace element geochemistry of ocean water during the Middle to Late Cambrian to better understand the paleoenvironmental conditions that dominated during that time interval, and
ii. To understand the associated changes of paleoredox conditions.

2. Geological setting

The Port au Port Group consists of mixed carbonate and siliciclastic sediments that crop out on the Port au Port Peninsula forming a belt approximately 400 km long and 75 km wide (Fig. 1; Williams, 1976, 1979; Chow and James, 1987). These deposits are a part of the autochthonous Cambro–Ordovician sequence (Upper Cambrian–Lower Ordovician shallow water carbonates changing into basinal shales) that comprise the tectono-stratigraphic Humber Zone of the northern Appalachian Orogen (Williams, 1976, 1979; Chow and James, 1987). The group is believed to represent shallow marine deposits on the outer part of a stable low-latitude shelf that bordered the Iapetus Ocean and reflects the gradual transition from Early Cambrian siliciclastic sediments to Early Ordovician carbonates (Fig. 2; Williams, 1976, 1979; Chow and James, 1987; Lavoie, 1994, 2008).

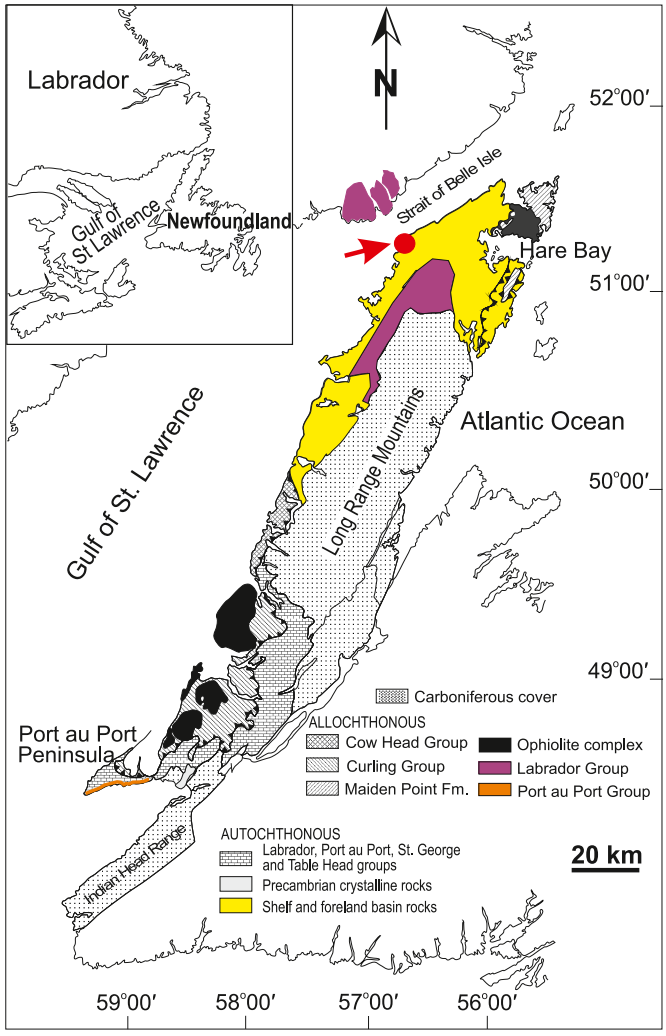

Fig. 1. Map of the study area showing the locations of the sampled core, NF-02 (Appendix 1) at the Strait of Belle Isle (51°30′00.0″ N; 56°29′56.0″ W), which spans the Port au Port Group carbonates in western Newfoundland, Canada (modified from Zhang and Barnes, 2004).

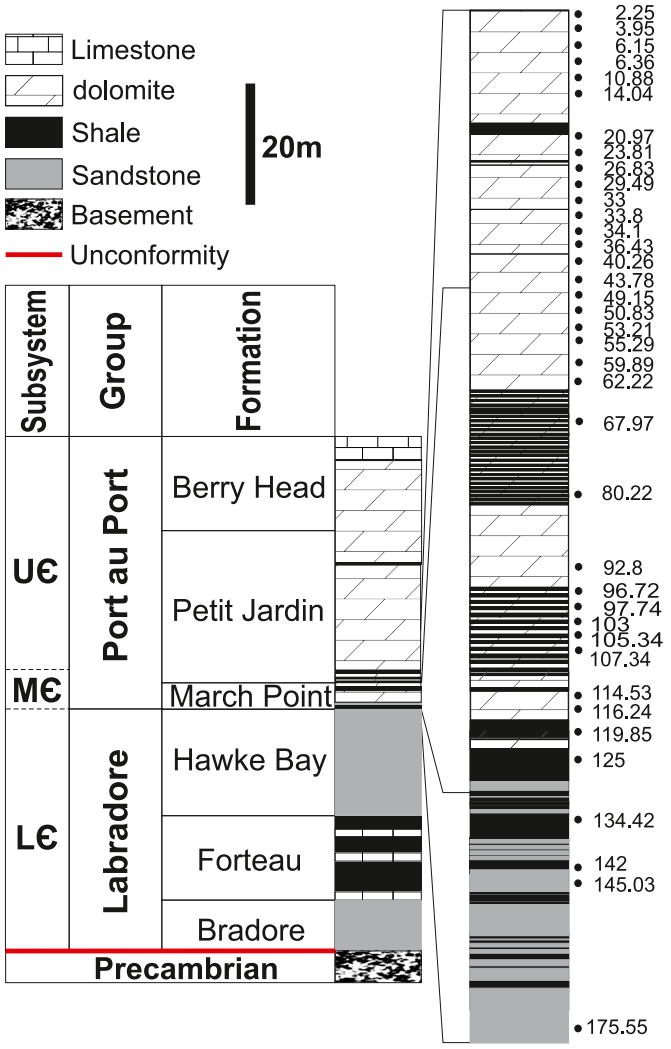

Fig. 2. Stratigraphic framework of the investigated dolomicrites from Belle Isle Strait in western Newfoundland, showing the approximate positions of investigated samples. The sample id refers to depth.

Uplift, faulting, and exposure on the Port au Port Peninsula during the Late Devonian Acadian Orogeny resulted in the development of karst topography on the exposed Cambrian and Ordovician carbonates (Dix, 1981). The Middle and Upper Cambrian shallow-marine strata of this part of the Humber Zone of the Appalachian Orogen (Williams, 1976, 1979) record the growth and demise of a continental margin of Iapetus. The paleographic reconstructions suggest that sediments on the outer part of the stable shelf were located at approximately 25° S, within the sub-tropical climate zone (Scotese et al., 1979). They comprise a part of an eastward-thickening prism of Lower Cambrian to Middle Ordovician volcanics, siliciclastics, and carbonates that rest uncomformably on the Grenvillian crystalline basement (Rodgers, 1968; Williams and Stevens, 1974; James and Steven, 1982).

3. Stratigraphy

3.1. Lithostratigraphy

Earlier field studies indicated that the Port au Port Group carbonates vary generally in lithology between laminated lime mudstones to packstones and oolitic grainstones (Chow and James, 1987). However, they are almost entirely dolomitized in the subsurface of the study area of Belle Isle Strait (Fig. 1; Core NF-02), dominated by microbial/peloidal

lime mudstones, and occasionally interbedded with shales (Fig. 2). The investigated dolostones in the sampled core NF-02 constitute the lower Port au Port Group (Fig. 2) that spans the uppermost Hawke Bay, entire March Point, and the lowermost Petit Jardin formations. The Petit Jardin Formation (only the lowermost ~47 m included in core NF-02) rests conformably on the March Point Formation (~83 m thick) since no unconformity surface has been documented yet between the March Point and the Hawke Bay formations (Fig. 2). The sampled carbonates consist mainly of laminated to massive gray dolomicrites with rare vugs that are entirely occluded with cements (Shembilu et al., 2021).

3.2. Biostratigraphy

There have been several studies on the Port au Port Group that were focused on the trilobite biostratigraphy. A preliminary age of late Middle to Late Cambrian was suggested in the 1930s by Schuchert and Dunbar (1934) and later studies (e.g., Whittington and Kindle, 1969; Boyce, 1977, 1979; Levesque, 1977; Stouge and Boyce, 1983) provided more details to date the various units of the succession (Fig. 3).

The trilobite biozonation scheme of the Petit Jardin Formation (Fig. 3) includes the *Cedaria*, *Crepicephalus*, *Dunderbagia, Elvina* and *Taenicephalus* zones, which span the Dresbachian to early Franconian stages of the regional (Laurentian) scheme of Upper Cambrian (Lochman, 1938; Troelsen, 1947; Levesque, 1977). There are three other biozones (the *Aphelaspis*, *Dicanthopyge*, and *Prehousia*; Levesque, 1977) that are compressed into a short interval between the *Crepicephalus* and *Dunderbergia* zones (Fig. 3), indicating a depositional break and/or condensed sedimentation near the Dresbachian-Franconian boundary

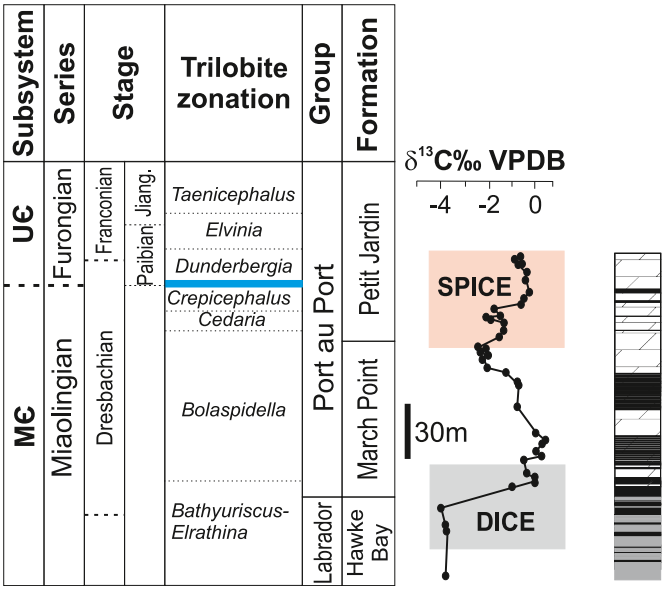

Fig. 3. The $\delta^{13}C$ profile of the investigated Middle–Upper Cambrian Belle Isle carbonates (from Shembilu and Azmy, 2021) and their trilobite biozonation scheme (after Lochman, 1938; Kindle and Whittington, 1965; Palmer, 1969; Levesque, 1977). The Blue line represents the compressed biozones (the *Aphelaspis, Dicanthopyge,* and *Prehousia*; Levesque, 1977). Legend as in Fig. 2. Detail in text. (For interpretation of the references to colour in this figure legend, the reader is referred to the Web version of this article.)

(Fig. 3), although no surface of unconformity can be physically recognized in the investigated core. The March Point Formation contains trilobites of the *Bathyuriscus-Elrathina* and *Bolaspidella* zones, which belong to late Middle Cambrian (Lochman, 1938; Levesque, 1977; Boyce, 1977). Trilobites gathered from the lower half of the underlying Hawke Bay Formation (*Bonnia-Olenellus* zone) correlate with the latest Early Cambrian (Boyce, 1977; Levesque, 1977). No fossils from the intervening *Plagiura-Poliella*, *Albertella* or *Glossopluera* zones (Early to Middle Cambrian) have yet been documented, which suggests that either the upper part of the Hawke Bay sandstones belongs to the lowermost Middle Cambrian or there is a hiatus (the Hawke Bay Event) at the Hawke Bay-March Point contact (Palmer and James, 1979).

4. Methodology

Samples were collected from Core NF-02 (Appendix 1, Fig. 1) that was drilled in the Strait of Belle Isle (51°30′00.0″ N, 56°29′56.0″ W), western Newfoundland. Sampling interval was generally between 30 cm and 2 m (Fig. 2) but the frequent occurrences of shale and sandstone interbeds (Fig. 2) made, in some cases, the sampling interval wider. The entire investigated interval spans the uppermost part (46 m) of the Hawke Bay Formation (lowermost Middle Cambrian) of the Labrador Group, the entire March Point Formation (83 m, Middle Cambrian) and the lowermost part (43 m) of the Petit Jardin Formation (uppermost Middle Cambrian) of the Port au Port Group (Fig. 2).

Thin sections of micritic carbonates were cut, stained with Alizarin Red-S and Potassium ferricyanide solutions (Dickson, 1966; Lindholm and Finkelman, 1972), and examined under standard polarizing microscope and cathodoluminoscope for petrographic features to identify the most micritic spots. A mirror-image slab of each thin section was also polished and cleaned with deionized water prior to microsampling for geochemical analyses. Cathodoluminescence (CL) was performed using a Technosyn cold cathodoluminoscope operated at ~12 kV accelerating voltage and ~0.7 mA gun current intensity.

The polished slabs were washed with deionized water and dried overnight at 45 °C. Approximately 10 mg were microsampled from the most micritic material in the cleaned slabs under a binocular microscope using a low-speed microdrill.

For elemental analyses (Appendix 1), the sample powder (~10 mg per sample) was digested in 2.5% (v/v) pure HNO_3 for 70–80 min and analyzed for major and trace elements using ICP-MS. The relative uncertainties of the measurement are better than 5% using BHV02 and internal standards. The calculations of major and trace element concentrations are based on an insoluble residue-free carbonates (100% soluble dolomite or calcite).

The Hawke Bay Formation is formed of sandstones and shales (Fig. 2) and the investigated uppermost part had few very thin highly argillaceous dolomite interbeds that were impossible to microsample enough carbonate material from them without contamination from siliciclastics and therefore were not run for trace element analyses.

5. Results

Petrographic examinations of the investigated carbonates indicate that they are dominated by fabric-retentive micritic to near-micritic dolostones (dolomicrites) that have insignificant organic matter. These dolostones consist of tightly packed, non-porous and planar crystals (4–35 μm) that exhibit non-CL (Fig. 4a and b; Shembilu and Azmy, 2021).

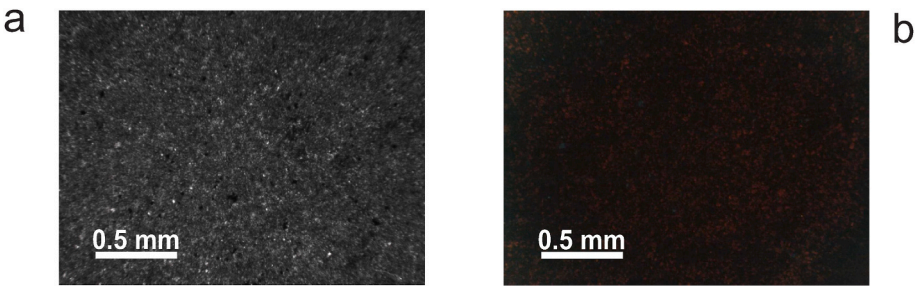

Fig. 4. Photomicrographs of (a) Dolomicrite (crossed polars: Sample 36.4), (b) CL image of (a).

Table 1
Summary of statistics of isotopic and trace element geochemical compositions of the investigated Belle Isle Strait carbonates of the Port au Port Group in western Newfoundland.

Sample ID	d13C ‰ VPDB	Sr (ppm)	Fe (ppm)	Mn (ppm)	Al (ppm)	P (ppm)	Ni (ppm)	Cu (ppm)	Th (ppm)	U (ppm)	V (ppm)	Mo (ppm)	∑REE (ppm)	Mn/ Sr	Th/ U	Mn/ Al	Fe/ Al
N	38	33	33	33	33	33	33	33	33	33	33	33	33	33	33	33	33
Mean	−1.2	90	21,465	857	13,133	280	12	7	2.14	0.83	18.79	1.05	45.2	10.4	2.7	0.20	3.7
Stdev	1.1	44	19,655	402	17,467	350	10	9	2.81	0.61	18.46	1.51	37.9	4.7	2.8	0.16	4.2
Max	0.3	264	83,975	2261	75,238	1697	39	36	10.73	2.39	79.35	7.16	154.3	26.9	8.3	0.63	22.3
Min	−3.9	30	4087	296	872	30	2	1	0.03	0.16	2.90	0.00	9.7	3.6	0.1	0.01	0.6

The concentrations of the paleoenvironmental proxies (e.g., Śliwiński et al., 2010; Pattan et al., 2013; Acharya et al., 2015; Liyuan et al., 2021), including P, Ni, Cu (bioproductivity), Al, ∑REE, Mn, Fe (weathering), and Th/U (paleoredox), are listed in Appendix 1 and their statistics are summarized in Table 1. Compared with the elemental compositions of the other slightly younger Upper Cambrian (Martin point; Wang and Azmy, 2020) and Cambrian-Ordovician boundary (GSSP, Green Point; Azmy et al., 2015) carbonates of neighboring basins in western Newfoundland, the Belle Isle carbonates have generally higher mean P, Ni, Th/U, Mn, and Fe concentrations but lower Sr although the mean ∑REE values are very comparable.

The Sr values (90 ± 44 ppm; Table 1; Appendix 1) have consistent positive correlations with their P ($R^2 = 0.05$), Ni ($R^2 = 0.16$), Cu ($R^2 = 0.01$), Al ($R^2 = 0.57$), total REE (∑REE; $R^2 = 0.35$), Th/U ($R^2 = 0.20$), Fe ($R^2 = 0.60$), and Mn ($R^2 = 0.32$) counterparts although some of the correlations seem week to insignificant (Fig. 5a–h).

An earlier C-isotope stratigraphic study (Shembilu and Azmy, 2021) indicated that the $\delta^{13}C$ profile of the Belle Isle succession documents two distinct negative excursions (Fig. 3). The individual profiles of the investigated paleoenvironmental proxies show also distinct and consistent positive shifts associated with those excursions on the $\delta^{13}C$ profile (Fig. 6).

6. Discussion

6.1. Evaluation of sample preservation

Petrographic examinations of the investigated Bell Isle carbonates reveal fabric-retentive textures and micritic (4 μm) to near-micritic (<35 μm) grainsize (Fig. 4a and b). The degree of alteration depends mainly on the water/rock interaction ratio and the extent of reset of the retained proxy signal (Veizer, 1983; Banner and Hanson, 1990). The dominant micritic to near-micritic grainsize and insignificant recrystallization of the investigated dolomicrites as well as their retention of sedimentary fabrics (Fig. 4a) argue for insignificant alteration (Shembilu and Azmy, 2021), which is consistent with their exhibited non-CL image (Fig. 4b). Luminescence in carbonates is mainly activated by high concentrations of Mn but quenched by high concentrations of Fe (Marshall, 1988; Machel and Burton, 1991; Budd et al., 2000). Although dull and non-CL images, at times, reflect preservation of primary geochemical signatures (e.g., Veizer et al., 1999), diagenetic carbonates such as late-burial cements may still exhibit dull to non-CL images due to their high Fe contents (Rush and Chafetz, 1990). Therefore, the CL results have to be taken with caution and confirmed by additional screening tests (Brand et al., 2011).

Burial Diagenesis of carbonates leads to a significant depletion in the Sr contents but enrichment of other elements such as Mn, Fe (Veizer, 1983) and ∑REE (Azmy et al., 2011) in the altered phase. However, The Sr concentrations of the Bell Isle carbonates exhibit positive correlations with Mn, Fe, and ∑REE as well as the other paleoenvironmental proxies (Fig. 5a–h), which are entirely opposite to the expected trends caused by diagenetic alteration.

Earlier studies suggested that diagenetic alteration of carbonates, under low water/rock interaction conditions (insignificant recrystallization/aggrading neomorphism), has insignificant influence on the contents of paleoenvironmental proxies such as P, Ni, Cu, Th and U (e.g., Veizer, 1983; Śliwiński et al., 2010; Pattan et al., 2013; Acharya et al., 2015; Wang and Azmy, 2020). Thus, the lack of diagenetic trend shown by the diagenetic proxies is consistent with the petrographic preservation and supports the retention of at least near-primary geochemical signatures of the paleoenvironmental proxies (e.g., Wang and Azmy, 2020).

This is also supported by the proxies' profiles (Fig. 6) that show distinct and consistent positive shifts associated with the negative excursions on the $\delta^{13}C$ profile (Fig. 6) since no diagenetic process has been known yet to cause such consistent changes.

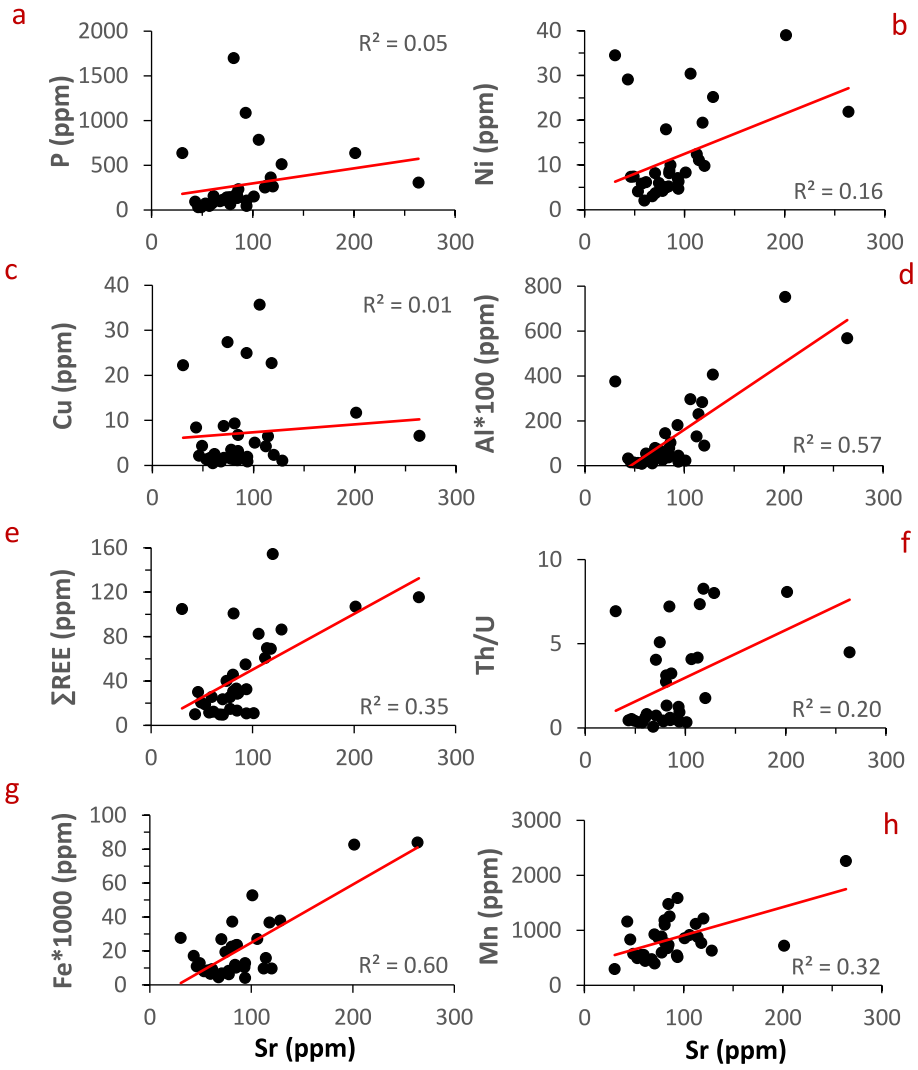

Fig. 5. Scatter diagrams showing correlations of Sr with (a) P, (b) Ni, (c) Cu, (d) Al, (e) ∑REE, (f) Th/U, (g) Fe, and (h) Mn of the investigated dolomicrites from the Port au Port Group.

6.2. Paleoenvironmental proxies

Variations in eustatic sealevel, particularly those related to time events, are commonly associated with changes in the $\delta^{13}C$ signatures and trace element concentrations of the marine carbonates due to changes in primary productivity, redox conditions, and impact of terrestrial material and nutrient inputs into the ocean (e.g., Wignall and Twitchett, 1996; Murphy et al., 2000; Kimura et al., 2005; Wignall et al., 2007; Piper and Calvert, 2009; Śliwiński et al., 2010; Dickson et al., 2011).

The C-isotope profile of the investigated Belle Isla carbonates (Shembilu and Azmy, 2021, Fig. 3) records a lower negative excursion (~4‰) that correlates with the Middle Cambrian global DICE (Drumian Carbon Isotope Excursion) event (Schmid, 2017) and an upper negative counterpart (~2‰) that correlates with the base of the lowermost Upper Cambrian global SPICE (Steptoean Positive Carbon Isotope Excursion) event (Pulsipher et al., 2021). The negative shift at the base of SPICE inflects into the positive SPICE excursion (Shembilu and Azmy, 2021). The correlations of these excursions were supported by the Middle–Upper Cambrian trilobite biozonation scheme and the negative shifts were possibly caused by brief sealevel falls (Babcock et al., 2015), along the Cambrian long-term sealevel rise (Landing and Ford, 2007, 2012a,b; Landing et al., 2010, 2011; Babcock et al., 2015), that brought down surface oxygenated water to oxidize buried organic matter and release light CO_2 enriched in ^{12}C (Shembilu and Azmy, 2021) although some earlier studies (e.g., Li et al., 2020) suggested that the DICE negative $\delta^{13}C$ excursion has been caused by inputs of upwelling anoxic deep waters, loaded with organic matter, into the oxic shallow water column during sea transgression.

Aluminum and REE are enriched in crustal rocks and therefore reflect the impact of the terrestrial inputs in oceans (e.g., Veizer, 1983; Śliwiński et al., 2010; Tripathy et al., 2014; Azmy et al., 2011; Wang and Azmy, 2020), which is confirmed by their considerable positive correlation ($R^2 = 0.57$; Appendix 1). The drop in sealevel likely exposed more

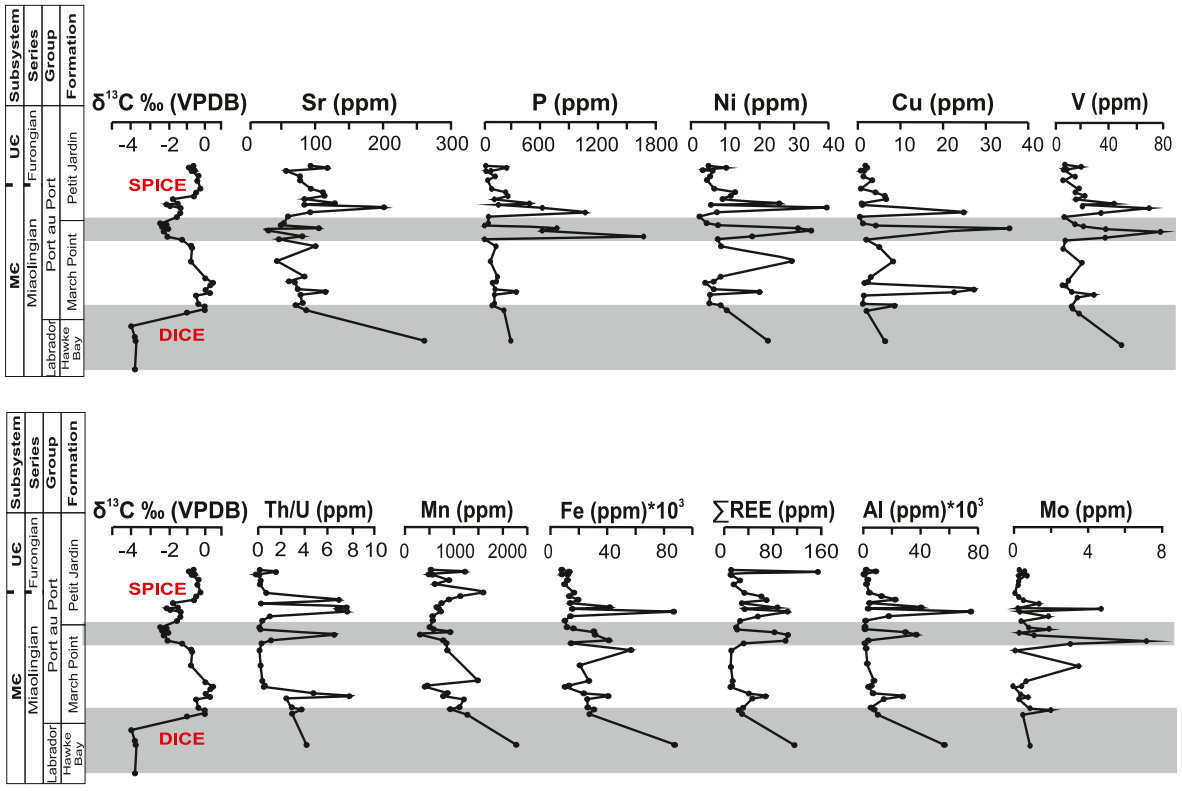

Fig. 6. The profiles of Sr, P, Ni, Cu, Th/U, ∑REE, Fe, Mn, Al, V, and Mo across the investigated Core NF-02 from the Belle Isle Strait succession. The $\delta^{13}C$ profile is from Shembilu and Azmy (2021).

land areas for weathering that enhanced the inputs of terrigenous material into ocean water and caused the positive shifts in the Al and ∑REE profiles, which are associated with both of the main negative $\delta^{13}C$ excursions (Fig. 6).

Phosphorus, Ni, and Cu are among the micronutrients and known to be reliable proxies for bioproductivity (e.g., Tribovillard et al., 2006; Arnaboldi and Meyers, 2007; Morel et al., 2004; Śliwiński et al., 2010). Their profiles reconstructed from the investigated carbonates (Fig. 6) exhibit similar positive shifts associated with the negative $\delta^{13}C$ excursions, thus suggesting a relative increase in nutrient inputs from land sources likely through riverine discharge during the drop in sealevel. This is consistent with the increase of terrigenous inputs during those periods, which is shown by the weathering (Al and ∑REE) proxy profiles (Fig. 6). Eustatic sealevel drop is associated with global cooling and well-mixed oceans, which suggests that input of nutrients was not restricted to land sources (riverine inputs of weathered material) but had contributions from upwelling. This agrees with the general low concentrations of V and Mo (Table 1; Appendix 1) and their consistent enrichments, as well as those of Ni, associated with the negative $\delta^{13}C$ excursions (Fig. 6) since these elements are known to be enriched in deep anoxic seawater (Crusius et al., 1996; Pagés and Schmid, 2016; Acharya et al., 2015).

Sealevel changes influence the oxygenation of water column and consequently the oxidation state of redox-sensitive elements and their solubility in seawater, which control their degree of enrichment in marine sediments (e.g., Wignall and Twitchett, 1996; Kimura et al., 2005; Arnaboldi and Meyers, 2007; Wignall et al., 2007). In oxidizing environments, uranium ions occur as $[U^{6+}]$ that form uranyl carbonate, which is soluble in water whereas in reducing conditions, they retain the lower oxidation state $[U^{4+}]$ and form the insoluble uranous fluoride which is trapped into marine carbonates (Wignall and Twitchett, 1996). In contrast, thorium is not affected by redox conditions in the water column and occurs permanently in the insoluble $[Th^{4+}]$. Thus, sediments of anoxic environments are richer in uranium and have lower Th/U than those of oxic environments. Therefore, the Th/U ratio has been used as a proxy for environmental redox conditions. The Th/U profile of the Belle Isle carbonates also exhibits positive shifts associated with the negative $\delta^{13}C$ excursions of both of the DICE and base of SPICE events. This implies a relative increase in oxygenation of water column, which is consistent with the suggested drop of sealevel (Shembilu and Azmy, 2021) and with the enhancement of inputs of terrigenous material due to the increase of land areas exposed to weathering. However, the correlated enrichment in Th/U in the current study does not support a scenario of anoxic/euxinic environment (e.g., Pagés and Schmid, 2016) or attributing the negative $\delta^{13}C$ shift, particularly that of the DICE event, to upwelling deep anoxic waters (rich in organic matter) onto oxic shallow inner shelf environments during sea transgression (e.g., Li et al., 2020) because U is expected to be enriched in the upwelling material (such as organic matter) and this would lead to general high U concentrations (e.g., Pagés and Schmid, 2016), which is not the case ([U] = 0.83 ± 0.61 ppm; Table 1).

The relative variations in Mn and Fe contents may reflect the changes in the redox conditions (Veizer et al., 1983; Landing and Bruland, 1987) because they are more soluble and enriched in seawaters in their lower

oxidation state (Mn^{+2} and Fe^{+2}, respectively) under dysoxic/anoxic conditions compared with oxic shallow water settings. The Mn and Fe contents of Belle Isle carbonates vary from 296 to 2261 ppm and 4087–83,975 ppm, respectively (Table 1), which are significantly higher than those of modern warm shallow-water marine carbonates (Mn = 5.4–30 ppm and Fe = 1–20 ppm, respectively; Ichukuni, 1973; Lorens, 1981; Brand et al., 2003). Manganese and Fe are also diagenetic proxies and become enriched with diagenetic alteration during progressive burial. However, the Mn and Fe profiles of the investigated carbonates exhibit unexpectedly consistent positive correlations ($R^2 = 0.3$ and 0.6, respectively) with Sr (Fig. 5) and also positive shifts correlated with the primary negative $\delta^{13}C$ excursions on the Belle Isle profile (Fig. 6), which suggest that the enrichment in those elements is very unlikely to be a diagenetic overprint. These elements are generally enriched in the siliciclastic crustal rocks (Fig. 2), such as feldspars, and the increase in terrigenous inputs, caused by active weathering, raised their concentrations in the waters. This is supported by the consistently correlated positive shifts exhibited by the profiles of weathering (e.g., Al and ∑REE) and nutrient (P, Ni and Cu) proxies.

On the other hand, Mn and Fe concentrations may still be used as redox proxies when normalized by Al to eliminate the influence of detrital fractions (Clarkson et al., 2014). The investigated Belle Isle carbonates have mean ratios of Mn/Al (0.20 ± 0.16; Table 1) and Fe/Al (3.7 ± 4.2; Table 1), which are significantly higher than those of the upper continental crust (0.0075 and 0.44, respectively; McLennan, 2001). This may reflect the occurrence of the Fe–Mn oxy-hydroxides (Pattan et al., 2013) that cannot form in anoxic environment but oxic, or at least dysoxic, conditions (cf. Landing et al., 2002; Pattan et al., 2013; Wang and Azmy, 2020).

The variations of the profiles of proxies, associated with the negative $\delta^{13}C$ excursions correlated with the top of DICE and base of the SPICE events, are comparable to those documented in association with a negative $\delta^{13}C$ excursion of the younger uppermost Cambrian HERB event (Hellnmaria – Red Tops Boundary) in western Newfoundland (Wang and Azmy, 2020). Those variations during the HERB event are deemed to be correlated with a possible short-term sealevel fall during the Late Cambrian (Wang and Azmy, 2020).

Although the $[Sr^{2+}]$ concentrations of the investigated dolomicrites are low (30–264 ppm) and comparable with those of the micritic carbonates in the neighboring basins (e.g., Azmy and Lavoie, 2009; Azmy, 2019a,b), the Sr profile still shows a consistent enrichment associated with the negative $\delta^{13}C$ excursions of the DICE and base of SPICE and with the correlated positive shifts by the weathering (Al and ∑REE), bioproductivity (P, Ni, and Cu) and redox (Th/U, Mn, and Fe) profiles. This is opposite to the trends expected from diagenetic alteration (Veizer, 1983). Therefore, the Sr behavior may reflect the influence of another factor such as the source of precursor lime mudstone that might have had contributions from primitive Cambrian aragonitic shells or alternations between aragonitic and calcitic seas. A similar pattern of [Sr] enrichment has been also documented in association with the younger uppermost Cambrian HERB event in the area (Wang and Azmy, 2020). The suggested sealevel falls (Shembilu and Azmy, 2021) could reflect brief global cooling events that led to conditions of relatively more oxygenated and well-mixed waters than those dominated during the Cambrian long-term rising sealevel. These conditions possibly favored the precipitation of some aragonitic mud, which is richer in Sr (Kitano and Oomori, 1971; Tucker and Wright, 2009) than calcite, particularly in shallow-warm tropical environment (Neilson et al., 2016). However, it is suggested that the interpretation of the correlated Sr enrichment has to be taken with caution till further studies may reveal more about the nature of those variations.

Aragonite loses U during alteration (Chen et al., 2018), which might have contributed to the Th/U ratios (redox proxy). Nevertheless, the geochemical evidence from the poor (positive) correlation of Sr with U contents ($R^2 = 0.15$; Appendix 1) and the diagenetic proxies (Fig. 5a–h) and petrographic preservation (Fig. 4a and b) argue against any influence of carbonate mineralogy through U contributions to the Th/U ratios but support at least near-primary Th/U ratios.

Earlier few studies on the ice free Cretaceous, similar to the proposed greenhouse Cambrian (e.g., Berner and Kothavala, 2001; Wotte et al., 2019), suggested that variations in global groundwater reservoir, by alternations between humid and arid climates, might cause eustatic sealevel fluctuations (Hay and Leslie, 1990; Wendler and Wendler, 2016; Wendler et al., 2016a,b), which may explain the sealevel changes but yet cannot be reconciled with the oxic intervals suggested by the paleoredox proxies (Th/U, Mn/Al, and Fe/Al).

An alternative scenario that may partially reconcile the consistent variations of the paleoenvironment proxies in the Belle Isle carbonates with sealevel rise during greenhouse Cambrian (e.g., Li et al., 2020) is that the negative $\delta^{13}C$ excursions were caused by enhanced atmospheric CO_2 inputs from volcanic or methanogenic sources that might have increased upwelling, anoxia, and nutrients (Saltzman and Thomas, 2012) and the enrichment of Al, ∑REE, Mn and Fe was caused by active chemical weathering during humid (wet) climate intervals while that of P, Ni, and Cu (Fig. 6) was by upwelling, which might have placed light organic carbon into the shallow oxic environment to enhance the negative $\delta^{13}C$ shifts (e.g., Li et al., 2020). Possible contributions from the weathered organic matter might have also contributed to those negative shifts. A comparable scenario of humid climates, which resulted in high inputs of weathered crustal material, has been suggested for the Late Permian (e.g., Li et al., 2021). However, this scenario cannot explain the correlated enrichments of Sr, Th/U ratios, or the high Mn/Al and Fe/Al ratios (0.20 ± 0.16 and 3.7 ± 4.2, respectively; Table 1), particularly when upwelling is generally stronger in well-mixed oceans during sealevel lowstands. Similarly, the scenario cannot be supported by the general low U, V and Mo contents in the Belle Isle carbonates.

7. Conclusions

- The petrographic and geochemical examinations of the investigated dolomicrites from the Belle Isle Strait reveal the preservation of at least near-primary trace element signatures that can be utilized as proxies to reconstruct the paleoenvironmental conditions (weathering, bioproductivity, and redox) during the Middle Cambrian DICE event and lowermost Upper Cambrian SPICE events.
- The correlated positive shifts on the Sr profile with their counterparts of the investigated paleoenvironmental proxies argue for the preservation of at least near-primary geochemical signatures.
- The profiles of weathering (Al and ∑REE), bioproductivity (P, Ni, and Cu), and redox (Th/U, Mn/Al, and Fe/Al) proxies exhibit consistent positive shifts associated with the negative $\delta^{13}C$ excursions, which are correlated with the DICE and base of the SPICE events documented by an earlier study. They reflect enhancement in the riverine inputs of weathered crustal rocks due to possible active weathering while the enrichment in the P, Ni, Cu, V, and Mo was likely by upwelling. These consistent positive shifts are consistent with possible brief sealevel falls during the Cambrian long-term sealevel rise.
- The positive shifts exhibited by the Mn and Fe profiles reflect the influence of terrigenous inputs rather than diagenesis, which is supported by the associated enrichment in the Mn/Al, and Fe/Al values and consistent with the correlated positive Th/U shifts.

Declaration of competing interest

The authors declare that they have no known competing financial interests or personal relationships that could have appeared to influence the work reported in this paper.

Appendix 1 Samples IDs, description, Formation, and isotopic and elemental geochemical compositions of Belle Isle carbonates. Sample number refers to depth. The $\delta^{13}C$ data are from Shembilu and Azmy (2021).

Sample id	Formation	d13CVPDB ‰	Sr (ppm)	Fe (ppm)	Mn (ppm)	Al (ppm)	P (ppm)	Ni (ppm)	Cu (ppm)	Th (ppm)	U (ppm)	V (ppm)	Mo (ppm)	La (ppm)	Ce (ppm)	Pr (ppm)	Nd (ppm)	Sm (ppm)	Eu (ppm)	Gd (ppm)	Tb (ppm)	Dy (ppm)	Ho (ppm)	Er (ppm)	Tm (ppm)	Yb (ppm)	Lu (ppm)	∑REE (ppm)
2.25	Petit Jardin	−0.6	94	4087	515	1879	44	4.6	1.9	0.15	0.40	4.04	0.24	2.36	4.87	0.51	1.89	0.31	0.08	0.30	0.04	0.21	0.04	0.11	0.02	0.10	0.01	10.85
3.95	Petit Jardin	−0.9	120	9681	1215	9002	261	9.8	2.4	1.95	1.10	17.07	0.42	31.14	77.59	7.40	25.86	3.61	0.70	3.24	0.39	1.82	0.35	0.95	0.14	0.96	0.14	154.32
6.15	Petit Jardin	−0.6	68	4490	476	1048	96	3.0	0.9	0.03	0.36	3.16	0.21	2.00	4.39	0.47	1.76	0.30	0.08	0.30	0.04	0.21	0.04	0.10	0.01	0.07	0.01	9.78
6.36	Petit Jardin	−0.8	57	8592	552	872	45	5.8	1.7	0.17	0.52	3.73	0.60	2.22	5.22	0.56	2.20	0.38	0.09	0.42	0.00	0.25	0.00	0.11	0.00	0.08	0.00	11.53
10.88	Petit Jardin	−0.5	78	8356	887	3501	142	5.1	1.5	0.30	0.68	10.14	0.15	4.53	11.17	1.23	4.75	0.92	0.24	0.89	0.14	0.73	0.14	0.35	0.05	0.32	0.04	25.48
14.04	Petit Jardin	−0.5	78	6307	596	2598	63	4.2	3.5	0.23	0.59	4.24	0.14	2.72	6.63	0.71	2.74	0.51	0.13	0.51	0.08	0.39	0.08	0.20	0.03	0.17	0.02	14.91
20.97	Petit Jardin	−0.3	94	12,891	1587	4547	104	6.3	0.9	0.73	0.78	13.78	0.00	5.33	13.73	1.57	6.22	1.28	0.36	1.31	0.22	1.21	0.23	0.59	0.08	0.47	0.07	32.67
23.81	Petit Jardin	−0.5	112	9648	1119	13,124	251	12.4	4.3	1.81	0.43	12.22	0.19	10.73	28.23	2.70	10.67	1.99	0.52	2.00	0.29	1.55	0.31	0.80	0.12	0.73	0.11	60.74
26.83	Petit Jardin	−0.7	114	15,884	881	23,058	274	11.1	6.5	6.39	0.87	19.49	0.44	13.97	30.56	3.38	12.61	2.18	0.49	2.10	0.30	1.61	0.33	0.90	0.13	0.85	0.12	69.53
29.49	Petit Jardin	−1.7	85	10,245	736	4706	133	8.7	6.8	0.99	2.13	12.75	1.29	5.79	12.66	1.39	5.25	0.91	0.20	0.96	0.12	0.63	0.11	0.30	0.00	0.27	0.00	28.58
33	Petit Jardin	−1.5	128	37,967	632	40,680	510	25.2	1.1	6.53	0.81	42.80	0.17	17.30	37.27	4.30	16.54	2.87	0.75	2.69	0.36	1.82	0.35	0.94	0.14	0.90	0.13	86.36
33.8	Petit Jardin	−2.1																										
34.1	Petit Jardin	−2.0	84	11,816	679	3743	178	5.2	1.2	1.18	0.16	16.71	4.68	6.13	15.16	1.65	6.29	1.12	0.23	1.12	0.00	0.74	0.00	0.35	0.00	0.31	0.00	33.10
36.43	Petit Jardin	−1.4	201	82,673	720	75,238	636	39.0	11.7	9.86	1.22	69.90	0.28	22.04	46.69	5.37	20.22	3.42	0.75	3.15	0.42	2.06	0.40	1.05	0.16	1.03	0.15	106.92
40.26	Petit Jardin	−1.4	93	10,439	547	18,173	1086	7.1	25.0	2.53	2.02	32.49	1.81	8.40	22.89	2.84	12.08	2.33	0.52	2.24	0.29	1.44	0.27	0.71	0.10	0.69	0.10	54.89
43.78	Petit Jardin	−1.5	60	6494	555	1912	72	2.0	0.5	0.18	0.29	3.57	0.41	4.83	11.57	1.21	4.67	0.83	0.20	0.87	0.12	0.61	0.12	0.30	0.04	0.27	0.04	25.69
49.15	Petit Jardin	−2.4	53	8023	494	1293	70	4.1	1.4	0.14	0.42	11.87	0.73	3.63	8.55	0.91	3.48	0.60	0.16	0.62	0.08	0.42	0.08	0.20	0.03	0.17	0.03	18.96
50.83	March Point	−2.2	49	12,883	573	1471	30	7.4	4.38	0.30	0.70	18.34	1.82	3.80	9.44	1.01	3.88	0.70	0.16	0.74	0.00	0.51	0.00	0.24	0.00	0.20	0.00	20.69
53.21	March Point	−2.2	106	27,129	913	29,695	783	30.4	35.7	3.22	0.79	36.09	0.24	13.28	35.34	4.14	17.05	3.28	0.86	3.10	0.43	2.19	0.42	1.06	0.15	0.98	0.14	82.42
55.29	March Point	−2.2	30	27,670	296	37,612	635	34.5	22.3	5.79	0.83	79.35	1.00	18.57	46.60	5.77	21.80	3.51	0.72	3.50	0.42	1.85	0.33	0.87	0.11	0.79	0.11	104.94
59.89	March Point	−2.0	81	37,293	770	3821	1697	17.9	9.3	0.84	0.64	35.72	7.16	16.36	39.95	5.69	23.33	4.54	1.07	4.39	0.57	2.50	0.41	0.96	0.11	0.76	0.09	100.72
62.22	March Point	−1.7	46	10,903	833	1557	31.1	7.3	2.2	0.32	0.60	4.28	3.01	6.10	12.52	1.66	6.14	0.99	0.24	0.92	0.13	0.63	0.12	0.30	0.04	0.26	0.04	30.07
67.97	March Point	−0.8	101	52,802	855	2363	150	8.3	5.1	0.17	0.51	2.90	0.00	2.04	4.70	0.57	2.20	0.39	0.09	0.39	0.05	0.27	0.05	0.13	0.02	0.12	0.02	11.04
80.22	March Point	−0.8	43	17,160	1160	3249	91	29.1	8.4	1.06	2.35	17.31	3.44	2.10	4.36	0.47	1.77	0.30	0.068	0.28	0.042	0.23	0.048	0.14	0.02	0.15	0.02	10.00
92.8	March Point	−0.1	85	23,306	1480	7829	165	8.2	3.2	1.09	1.81	7.49	0.57	2.76	5.65	0.66	2.53	0.42	0.096	0.39	0.055	0.28	0.057	0.16	0.02	0.16	0.02	13.27
96.72	March Point	0.3	61	9365	443	5422	154	6.1	2.6	0.54	0.65	5.05	0.36	2.33	5.26	0.63	2.46	0.43	0.10	0.38	0.06	0.29	0.06	0.16	0.02	0.16	0.02	12.38
97.74	March Point	0.2	71	6732	397	4200	113	3.7	1.7	0.44	0.60	3.83	0.00	1.90	4.11	0.50	1.88	0.32	0.08	0.29	0.04	0.23	0.05	0.13	0.02	0.12	0.02	9.70

(*continued on next page*)

(*continued*)

Sample id	Formation	d13CVPDB ‰	Sr (ppm)	Fe (ppm)	Mn (ppm)	Al (ppm)	P (ppm)	Ni (ppm)	Cu (ppm)	Th (ppm)	U (ppm)	V (ppm)	Mo (ppm)	La (ppm)	Ce (ppm)	Pr (ppm)	Nd (ppm)	Sm (ppm)	Eu (ppm)	Gd (ppm)	Tb (ppm)	Dy (ppm)	Ho (ppm)	Er (ppm)	Tm (ppm)	Yb (ppm)	Lu (ppm)	∑REE (ppm)
103	March Point	−0.1	74	19,410	866	7147	140	5.9	27.4	1.58	0.31	9.19	0.31	6.64	16.59	2.25	8.77	1.56	0.37	1.40	0.20	1.02	0.19	0.48	0.07	0.43	0.06	40.03
105.34	March Point	0.1	118	36,831	770	28,325	363	19.4	22.7	5.68	0.69	26.54	0.70	14.58	29.52	3.41	12.98	2.25	0.54	2.06	0.28	1.46	0.28	0.75	0.11	0.74	0.11	69.06
107.34	March Point	−0.6	81	22,259	1184	14,491	134	5.0	1.5	1.86	0.68	13.87	0.21	8.38	19.47	2.61	9.87	1.57	0.35	1.44	0.18	0.85	0.16	0.38	0.05	0.33	0.05	45.69
114.53	March Point	−0.4	81	22,550	1101	5729	135	4.9	1.4	0.98	0.31	9.11	0.76	6.11	13.01	1.54	5.92	1.06	0.23	1.05	0.14	0.73	0.13	0.35	0.00	0.32	0.00	30.58
116.24	March Point	−0.1	70	26,951	927	7933	109	8.2	8.8	1.16	0.29	9.68	1.94	4.54	10.10	1.21	4.59	0.82	0.19	0.81	0.11	0.53	0.10	0.26	0.00	0.25	0.03	23.55
119.85	March Point	−0.1	86	23,528	1254	10,327	231	10.0	2.1	1.76	0.54	15.03	0.42	6.14	12.44	1.44	5.51	0.94	0.24	0.88	0.12	0.62	0.12	0.33	0.05	0.31	0.05	29.19
125	March Point	−0.5																										
134.42	Hawke Bay	−3.9																										
142	Hawke Bay	−3.7																										
145.03	Hawke Bay	−3.6	264	83,975	2261	56,847	306	21.9	6.6	10.73	2.39	48.48	0.82	27.88	55.26	5.40	17.32	2.16	0.63	2.24	0.29	1.54	0.33	1.00	0.16	1.12	0.17	115.50
175.55	Hawke Bay	−3.7																										

Acknowledgements

The authors want to thank Dr. Claudio Garbelli and an anonymous reviewer for their constructive reviews. Also, the efforts of Dr. I. Al-Aasm (editor) are much appreciated. Special thanks to Drs. J. Potter and B. Guéguen for their help with the geochemical analyses. This project was supported by funding (to Karem Azmy) from MITACS and the Petroleum Exploration Enhancement Program (PEEP), NL, Canada.

References

Acharya, S.S., Panigrahi, M.K., Gupta, A.K., Tripathy, S., 2015. Response of trace metal redox proxies in continental shelf environment: the Eastern Arabian Sea scenario. Continent. Shelf Res. 106, 70–84.

Arnaboldi, M., Meyers, P.A., 2007. Trace elements indicators of increased primary production and decreased water-column ventilation during deposition of latest Pliocene sapropels at five locations across the Mediterranean Sea. Palaeogeogr. Palaeoclimatol. Palaeoecol. 249, 425–443.

Azmy, K., Lavoie, D., 2009. High-resolution isotope stratigraphy of the Lower Ordovician St. George Group of western Newfoundland, Canada: implications for global correlation. Can. J. Earth Sci. 46, 1–21.

Azmy, K., Brand, U., Sylvester, P., Gleeson, S.A., Logan, A., Bitner, M.A., 2011. Biogenic and abiogenic low-Mg calcite (bLMC and aLMC): evaluation of seawater-REE composition, water masses and carbonate diagenesis. Chem. Geol. 280 (1–2), 180–190.

Azmy, K., Kendall, K., Brand, U., Stouge, S., Gordon, G.W., 2015. Redox conditions across the Cambrian-Ordovician boundary: elemental and isotopic signatures retained in the GSSP carbonates. Palaeoegeography, Palaeoclimatology, Palaeoecology 440, 440–454.

Azmy, K., 2019a. Carbon-isotope stratigraphy of the uppermost Cambrian in eastern Laurentia: implications for global correlation. Geol. Mag. 156 (5), 759–771.

Azmy, K., 2019b. Carbon-isotope stratigraphy of the SPICE event (Upper Cambrian) in eastern Laurentia: implications for global correlation and a potential reference section. Geol. Mag. 156 (8), 1311–1322.

Babcock, L.E., Peng, S.C., Brett, C.E., Zhu, M.Y., Ahlberg, P., Bevis, M., Robison, R.A., 2015. Global climate, sea level cycles, and biotic events in the Cambrian Period. Palaeoworld 24 (1–2), 5–15.

Banner, J.L., Hanson, G.N., 1990. Calculation of simultaneous isotopic and trace element variations during water-rock interaction with applications to carbonate diagenesis. Geochem. Cosmochim. Acta 54 (11), 3123–3137.

Berner, R.A., Kothavala, Z., 2001. GEOCARB III: a revised model of atmospheric CO_2 over Phanerozoic time. Am. J. Sci. 301, 182–204.

Boyce, W.D., 1977. New Cambrian Trilobites from Western Newfoundland: Unpublished B.Sc. Thesis. Memorial University of Newfoundland, p. 66.

Boyce, W.D., 1979. Further Developments in Western Newfoundland Biostratigraphy. Mineral Development Division, Department of Mines and Energy, Government of Newfoundland and Labrador. Report 79-1, 7–10.

Brand, U., Logan, A., Hiller, N., ichardson, J., 2003. Geochemistry of modern brachiopods: applications and implications for oceanography and paleoceanography. Chem. Geol. 198, 305–334.

Brand, U., Logan, A., Bitner, M.A., Griesshaber, E., Azmy, K., Buhl, D., 2011. What is the ideal proxy of Paleozoic seawater? Memories Ass. Australasian Palaeontol. Soc. Memories 41, 9–24.

Buatois, L.A., Mangano, M.G., Olea, R.A., Wilson, M.A., 2016. Decoupled evolution of soft and hard substrate communities during the cambrian explosion and great ordovician biodiversification event. Proc. Natl. Acad. Sci. U.S.A. 113 (25), 6945-8.

Budd, D.A., Hammes, U., Ward, W.B., 2000. Cathodoluminiscence in calcite cements: new insights on Pb and Zn sensitizing, Mn activation and Fe at low trace-element concentration. J. Sediment. Res. 70 (1), 217–226.

Chang, X., Hou, M., Woods, A., Chen, Z.Q., Liu, X., Liao, Z., Liu, Y., Chao, H., 2021. Late ordovician paleoceanographic change: sedimentary and geochemical evidence from northwest tarim and middle yangtze region, China. Palaeogeogr. Palaeoclimatol. Palaeoecol. 562, 110070.

Chen, X., Romaniello, S.J., Herrmann, A.D., Hardisty, D., Gill, B.C., Anbar, A.D., 2018. Diagenetic effects on uranium isotope fractionation in carbonate sediments from the Bahamas. Geochem. Cosmochim. Acta 237, 294–311.

Chow, N., James, N.P., 1987. Cambrian grand cycles: a northern appalachian perspective. Geol. Soc. Am. Bull. 98, 418–429.

Chow, N., James, N.P., 1992. Synsedimentary diagenesis of Cambrian peritidal carbonates: evidence from hardgrounds and surface paleokarst in the Port au Port Group, western Newfoundland. Bull. Can. Petrol. Geol. 40 (2), 115–127.

Clarkson, M.O., Poulton, S.W., Wood, R.A., 2014. Assessing the utility of Fe/Al and Fe-speciation to record water column redox conditions in carbonate-rich sediments. Chem. Geol. 382, 111–122.

Crusius, J., Calvert, S., Pedersen, T., Sage, D., 1996. Rhenium and molybdenum enrichments in sediments as indicators of oxic, suboxic and sulfidic conditions of deposition. Earth Planet Sci. Lett. 145, 65–78.

Derry, L.A., Kaufman, A.J., Jacobsen, S.B., 1992. Sedimentary cycling and environmental change in the Late Proterozoic: evidence from stable and radiogenic isotopes. Geochem. Cosmochim. Acta 56 (3), 1317–1329.

Dickson, A.J., Cohen, A.S., Coe, A.L., 2011. Seawater oxygenation during the paleocene-eocene thermal maximum. Geology 40 (7), 639–642.

Dickson, J.A.D., 1966. Carbonate identification and genesis as revealed by staining. J. Sediment. Res. 36 (2), 491–505.
Dix, G.R., 1981. The Codroy Group (Upper Mississippian) on the Port au Port Peninsula, western Newfoundland: stratigraphy, paleontology, sedimentology and diagenesis: unpublished M.Sc thesis. Memorial University of Newfoundland, p. 218.
Hay, W.W., Leslie, M.A., 1990. Could possible changes in global groundwater reservoir cause eustatic sea-level fluctuations? Sea-level change 161–170.
Hill, A.C., Walter, M.R., 2000. Mid-Neoproterozoic (~830–750 Ma) isotope stratigraphy of Australia and global correlation. Precambrian Res. 100, 181–211.
Ichukuni, M., 1973. Partition of strontium between calcite and solution: effect of substitution by manganese. Chem. Geol. 11, 315–319.
James, N.P., Steven, R.K., 1982. Anatomy and Evolution of a Lower Paleozoic Continental Margin. In: Western Newfoundland: 11th International Congress on Sedimentology, 2B. Field Guidebook, Hamilton, p. 75.
Kaufman, A.J., Jacobsen, S.B., Knoll, A.H., 1993. The Vendian record of Sr and C isotopic variations in seawater: implications for tectonics and paleoclimate. Earth Planet Sci. Lett. 120, 409–430.
Kimura, H., Azmy, K., Yamamuro, M., Zhi-Wen, J., Cizdziel, J.V., 2005. Intergrated stratigraphy of the Upper Proterozoic succession in Yunnan of South China: Re-evaluation of global correlation and carbon cycle. Precambrian Res. 138, 1–36.
Kindle, C.H., Whittington, H.B., 1965. New Cambrian and Ordovician fossil localities in western Western Newfoundland. Geol. Soc. Am. Bull 76, 683–688.
Kitano, Y., Oomori, T., 1971. The coprecipitation of uranium with calcium carbonate. J. Oceanogr. Soc. Jpn. 27 (1), 34–42.
Land, L.S., 1992. The dolomite problem: stable and radiogenic isotope clues. In: Isotopic Signatures and Sedimentary Records, Lecture Notes in Earth Sciences, vol. 43, pp. 49–68.
Landing, E., 2007. Ediacaran–Ordovician of east Laurentia–geologic setting and controls on deposition along the New York Promontory. In: Landing, E. (Ed.), S. W. Ford Memorial Volume: Ediacaran–Ordovician of East Laurentia, vol. 510. New York State Museum Bulletin, pp. 5–24.
Landing, E., 2012a. Time-specific black mudstones and global hyperwarming on the Cambrian–Ordovician slope and shelf of the Laurentia palaeocontinent. Palaeogeogr. Palaeoclimatol. Palaeoecol. 367–368, 256–272.
Landing, E., 2012b. The great American carbonate bank in eastern Laurentia: its births, deaths, and linkage to paleooceanic oxygenation (early cambrian–late ordovician). In: Derby, J.R., Fritz, R.D., Longacre, S.A., Morgan, W.A., Sternbach, C.A. (Eds.), The Great American Carbonate Bank: the Geology and Economic Resources of the Cambrian–Ordovician Sauk Megasequence of Laurentia, vol. 98. American Association of Petroleum Geologists Memoir, pp. 451–492.
Landing, W.M., Bruland, K.W., 1987. The contrasting biogeochemistry of iron and manganese in the Pacific Ocean. Geochem. Cosmochim. Acta 51 (1), 29–43.
Landing, E., Geyer, G., Bartowski, K.E., 2002. Latest Early Cambrian small shelly fossils, trilobites, and Hatch Hill dysaerobic interval on the Quebec continental slope. J. Paleontol. 76 (2), 287–305.
Landing, E., Westrop, S.R., Miller, J.F., 2010. Globally practical base for the uppermost Cambrian (Stage 10): FAD of the conodont Eoconodontus notchpeakensis and the Housian [sic, read 'Lawsonian' as the abstract text] Stage. In: Fatka, O., Budil, P. (Eds.), The 15th Field Conference of the Cambrian Stage Subdivision Working Group. Abstracts and Excursion Guide, Prague, Czech Republic and South-Eastern Germany, vol. 18. Czech Geological Survey, Prague.
Landing, E., Westrop, S.R., Adrain, J.M., 2011. The Lawsonian Stage – the Eoconodontus notchpeakensis FAD and HERB carbon isotope excursion define a globally correlatable terminal Cambrian stage. Bull. Geosci. 86, 621–640.
Lavoie, D., 1994. Diachronous tectonic collapse of the Ordovician continental margin, eastern Canada: comparison between the Quebec Reentrant and St. Lawrence Promontory. Can. J. Earth Sci. 31 (8), 1309–1319.
Lavoie, D., 2008. Appalachian foreland basin of Canada. 1-Canada. In: Miall, A.D. (Ed.), Sedimentary Basins of the United States and Canada. Elsevier Science Publishing, pp. 63–105.
LeRoy, M.A., Gill, B.C., Sperling, E.A., McKenzie, N.R., Park, T.-Y.S., 2021. Variable redox conditions as an evolutionary driver? A multi-basin comparison of redox in the middle and later Cambrian oceans (Drumian-Paibian). Palaeogeogr. Palaeoclimatol. Palaeoecol. 566, 1–16.
Levesque, R.J., 1977. Stratigraphy and Sedimentology of Middle Cambrian to Lower Ordovician Shallow Water Carbonate Rocks, Western Newfoundland: Unpublished M.Sc. Thesis. Memorial University of Newfoundland, p. 276.
Li, Q., Azmy, K., Yang, S., Xu, S.L., Yang, D., Zhang, X.H., Chen, A.Q., Chen, H.D., 2021. Early–Middle Permian strontium isotope stratigraphy of marine carbonates from the northern marginal areas of South China: controlling factors and implications. Geol. J. https://doi.org/10.1002/gj.4010.
Li, D., Zhang, X., Zhang, X., Zhu, H., Peng, S., Shen, Y., Sun, L., 2020. A paired carbonate–organic $\delta^{13}C$ approach to understanding the Cambrian Drumian carbon isotope excursion (DICE). Precambrian Res. 349, 105503.
Li, D., Zhang, X., Zhang, X., Zhu, H., Peng, S., Sun, L., Shen, Y., 2020. A paired carbonate-organic $\delta^{13}C$ approach to understanding the Cambrian Drumian carbon isotope excursion (DICE). Precambrian Res. 319, 105503.
Liang, T., Jones, B., 2021. Characteristics of primary rare earth elements and yttrium in carbonate rocks from the Mesoproterozoic Gaoyuzhuang Formation, North China: implications for the depositional system. Sediment. Geol. 415, 105864.
Lindholm, R.C., Finkelman, R.B., 1972. Calcite staining: semiquantitative determination of ferrous iron. J. Sediment. Petrol. 42, 239–242.
Liyuan, W., Qingjun, G., Changqiu, Z., Rongfei, W., Yinan, D., Xiaokun, H., Liyan, T., Jing, K., Xi, Y., 2021. Trace and rare earth elements geochemistry of sedimentary rocks in the Ediacaran-Cambrian transition from the Tarim Basin, Northwest China: constraints for redox environments. Precambrian Res. 352, 105942.
Lochman, C., 1938. Middle and upper cambrian fauna from western Newfoundland. J. Paleontol. 12, 461–477.
Lorens, R.B., 1981. Sr, Cd, Mn, and Co distribution coefficients in calcite as a function of calcite precipitation rate. Geochem. Cosmochim. Acta 45, 553–561.
McKirdy, D.M., Burgess, J.M., Lemon, N.M., Yu, X., Cooper, A.M., Costin, V.A., 2001. A chemostratigraphic overview of the late cryogenian interglacial sequence in the adelaide fold thrust belt, south Australia. Precambrian Res. 106, 149–186.
Machel, H.G., Burton, E.A., 1991. Factors governing cathodoluminescence in calcite and dolomite, and their implications for studies of carbonate diagenesis. Luminescence microscopy and spectroscopy, qualitative and quantitative applications. SEPM Short. Course 25, 37–57.
Marshall, D.J., 1988. Cathodoluminescence of Geological Materials. Unwin Hyman, Boston, p. 146.
McLennan, S.M., 2001. Relationships between the trace element composition of sedimentary rocks and upper continental crust. G-cubed 2 (4).
Morel, F.M.M., Milligan, A.J., Saito, M.A., 2004. Marine bioinorganic chemistry: the role of trace metals in the oceanic cycles of major nutrients. The Oceans and Marine Geochemistry. Treatise Geochem. 6, 113–143.
Murphy, A.E., Sageman, B.B., Hollander, D.J., Lyons, D.J., Brett, C.E., 2000. Black shale deposition and faunal overturn in the Devonian Appalachian basin: clastic starvation, seasonal water-column mixing, and efficient biolimiting nutrient recycling. Paleoceanography 15, 280–291.
Neilson, J.E., Brasier, A.T., North, C.P., 2016. Primary aragonite and high-Mg calcite in the late Cambrian (Furongian). Potential evidence from marine carbonates in Oman. Terra. Nova 28 (5), 306–315.
Pagés, A., Schmid, S., 2016. Euxinia linked to the Cambrian Drumian isotope excursion in Australia: geochemical and chemostratigraphic evidence. Paléo 3 461, 65–76.
Palmer, A.R., 1969. Cambrian trilobite distributions in North America and their bearing on Cambrian paleogeography of Newfoundland. Am. Assoc. Petrol. Geol. Mem. 12, 139–144.
Palmer, A.R., James, N.P., 1979. The Hawke Bay Event: a Circum-Iapetus Regression Near the Lower-Middle Cambrian Boundary: I. G.C.P. Meeting, Blacksburg, Virginia, p. A3.
Pattan, J.N., Mir, I.A., Parthiban, G., Karapurkar, S.G., Matta, V.M., Naidu, P.D., Naqvi, S.W.A., 2013. Coupling between suboxic condition in sediments of the western Bay of Bengal and southwest monsoon intensification: a geochemical study. Chem. Geol. 343, 55–66.
Piper, D.Z., Calvert, S.E., 2009. A marine biogeochemical perspective on black shale deposition. Earth Sci. Rev. 95, 63–96.
Pulsipher, A.P., Schiffbauer, J.D., Jeffrey, M.J., Huntley, J.W., Fike, D.A., Shelton, K.L., 2021. A Meta-Analysis of the Steptoean Positive Carbon Isotope Excursion: the SPICEraq Database. Earth-Science Reviews, p. 103442.
Rodgers, J., 1968. The eastern edge of the north American continent during the cambrian and early ordovician. In: Studies of Appalachian Geology: Northern and Maritime. John Wiley & Sons, New York, pp. 141–150.
Rush, P.F., Chafetz, H.S., 1990. Fabric retentive, non-luminescent brachiopods as indicators of original $\delta^{13}C$ and $\delta^{18}O$ compositions: a test. J. Sediment. Petrol. 60, 968–981.
Saltzman, M.R., Thomas, E., 2012. Carbon isotope stratigraphy. In: Gradstein, F., Ogg, J., Schmitz, M.D., Ogg, G. (Eds.), The Geologic Time Scale 2012, pp. 207–232.
Schmid, S., 2017. Chemostratigraphy and palaeoenvironmental characterization of the cambrian stratigraphy in the amadeus basin, Australia. Chem. Geol. 451, 169–182.
Schuchert, C., Dunbar, C.O., 1934. Stratigraphy of Western Newfoundland, vol. 1. Geological Society of America Memoir, p. 123.
Scotese, C.R., Bambach, R.K., Van der Voo, R., Zeigler, A.M., 1979. Paleozoic base maps. J. Geol. 87, 217–268.
Shembilu, N., Azmy, K., Blamey, N., 2021. Origin of middle–upper cambrian dolomites in eastern Laurentia: a case study from Belle Isle Strait, western Newfoundland. Mar. Petrol. Geol. 125, 104858.
Shembilu, N., Azmy, K., 2021. Carbon-isotope stratigraphy of the Middle–Upper Cambrian in eastern Laurentia: implications for global correlation. Mar. Petrol. Geol. 128, 105052.
Sholkovitz, E.R., Shen, G.T., 1995. The incorporation of rare-earth elements in modern coral. Geochem. Cosmochim. Acta 59, 2749–2756.
Śliwiński, M.G., Whalen, M.T., Day, J., 2010. Trace element variations in the Middle Frasnian Punctata Zone (Late Devonian) in the western Canada sedimentary basin-Changes in oceanic bioproductivity and paleoredox spurred by a pulse of terrestrial afforestation? Geol. Belg. 4, 459–482.
Stouge, S., Boyce, W.D., 1983. Fossils of Northwestern Newfoundland and Southeastern Labrador: Conodonts and Trilobites. Mineral Development Division, Department of Mines and Energy, Government of Newfoundland and Labrador. Report 83-3, 55.
Tribovillard, N., Algeo, T.J., Lyons, T., Riboulleau, A., 2006. Trace metals as paleoredox and paleoproductivity proxies: an update. Chem. Geol. 232, 12–32.
Tripathy, G.R., Singh, S.K., Ramaswamy, V., 2014. Major and trace element geochemistry of Bay of Bengal sediments: implications to provenances and their controlling factors. Palaeogeogr. Palaeoclimatol. Palaeoecol. 397, 20–30.
Troelsen, J.C., 1947. Geology of the Bonne Bay-Trout River Area. Unpublished Ph.D. thesis. Yale University, Newfoundland, p. 289.
Tucker, M.E., Wright, V.P., 2009. Carbonate Sedimentology. John Wiley & Sons.
Veizer, J., 1983. Chemical diagenesis of carbonates: theory and application of trace elements technique. In: Arthur, M.A., Anderson, T.F., Kaplan, I.R., Veizer, J., Land, L. S. (Eds.), Stable Isotopes in Sedimentary Geology, vol. 10. Society of Economic Paleontologists and Mineralogists (SEPM), Short course Notes, pp. 3.1–3.100.
Veizer, J., Compston, W., Clauer, N., Schidlowski, M., 1983. $^{87}Sr/^{86}Sr$ in Late Proterozoic carbonates: evidence for a "mantle" event at~ 900 Ma ago. Geochem. Cosmochim. Acta 47 (2), 295–302.

Veizer, J., Ala, D., Azmy, K., Bruckschen, P., Bruhn, F., Buhl, D., Carden, G.A.F., Diener, A., Ebneth, S., Godderis, Y., Jasper, T., Korte, C., Pawellek, F., Podlaha, O.G., Strauss, H., 1999. $^{87}Sr/^{86}Sr$, $\delta^{18}O$ and $\delta^{13}C$ evolution of Phanerozoic seawater. Chem. Geol. 161, 59–88.

Wang, L., Azmy, K., 2020. Palaeoenvironmental changes in slope carbonates across the late cambrian–early ordovician in western Newfoundland. Geol. J. 55 (5), 1–13.

Weaver, F.J., Macko, S.A., 1988. Source rocks of western Newfoundland. Organic Geochemistry In Petroleum Exploration 13, 411–421.

Wendler, J.E., Wendler, I., 2016. What drove sea-level fluctuations during the mid-Cretaceous greenhouse climage? Palaeogeogr. Palaeoclimatol. Palaeoecol. 441, 412–419.

Wendler, I., Wendler, J.E., Clarke, L.J., 2016a. Sea-level reconstruction for Turonian sediments from Tanzania based on integration of sedimentology, microfacies, geochemistry and micropaleontology. Palaeogeogr. Palaeoclimatol. Palaeoecol. 441, 564–578.

Wendler, J.E., Wendler, I., Vogt, C., Kuss, J., 2016b. Link between cyclic eustatic sea-level change and continental weathering: evidence for aquifer-eustasy in the Creatacous. Palaeogeogr. Palaeoclimatol. Palaeoecol. 441, 430–437.

Whittington, H.B., Kindle, C.H., 1969. Cambrian and ordovician stratigraphy of western Newfoundland. In: Kay, M. (Ed.), North Atlantic Geology and Continental Drift, vol. 12. American Association of Petroleum Geologists Memoir, pp. 655–664.

Wignall, P.B., Twitchett, R.J., 1996. Oceanic anoxia and the end Permian mass extinction. Science 272, 1155–1158.

Wignall, P.B., Zonneveld, J.P., Newton, R.J., Amor, K., Sephton, M.A., Hartley, S., 2007. The end Triassic mass extinction record of Williston Lake, British Columbia. Palaeogeogr. Palaeoclimatol. Palaeoecol. 253, 385–406.

Williams, H., Stevens, R.K., 1974. The ancient continental margin of eastern North America. In: The Geology of Continental Margins. Springer, Berlin, Heidelberg, pp. 781–796.

Williams, H., 1976. Tectonic Stratigraphic Subdivision of the Appalachian Orogen (Abstract), vol. 8. Geological Society of America, with Programs, p. 300.

Williams, H., 1979. Appalachian orogen in Canada. Can. J. Earth Sci. 16, 792–807.

Wotte, T., Skovsted, C.B., Whitehouse, M.J., Kouchinsky, A., 2019. Isotopic evidence for temperate oceans during the Cambrian explosion. Sci. Rep. 9, 1–9. https://doi.org/10.1038/s4518-019-42719-4.

Zhang, S., Barnes, C.R., 2004. Arenigian (Early Ordovician) sea-level history and the response of conodont communities, western Newfoundland. Can. J. Earth Sci. 41 (7), 843–865.